Edge Structural Stability and Kinetics of Graphene Chemical Vapor Deposition Growth

Haibo Shu,[†,‡] Xiaoshuang Chen,[†,*] Xiaoming Tao,[‡,*] and Feng Ding[†,‡,*]

[†]National Laboratory for Infrared Physics, Shanghai Institute of Technical Physics, Chinese Academy of Sciences, Shanghai 200083, China and [‡]Institute of Textiles and Clothing, Hong Kong Polytechnic University, Hong Kong, China

ABSTRACT

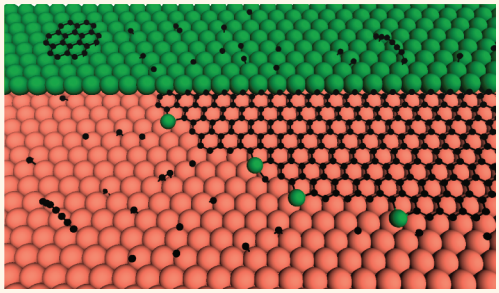

The energetics and growth kinetics of graphene edges during CVD growth on Cu(111) and other catalyst surfaces are explored by density functional theory (DFT) calculations. Different from graphene edges in vacuum, the reconstructions of both armchair (AC) and zigzag (ZZ) edges are energetically less stable because of the passivation of the edges by the catalytic surface. Furthermore, we predicated that, on the most used Cu(111) catalytic surface, each AC-like site on the edge is intended to be passivated by a Cu atom. Such an unexpected passivation significantly lowers the barrier of incorporating carbon atoms onto the graphene edge from 2.5 to 0.8 eV and therefore results in a very fast growth of the AC edge. These theoretical results are successfully applied to explain the broad experimental observations that the ZZ egde is the dominating edge type of growing graphene islands on a Cu surface.

KEYWORDS: graphene · chemical vapor deposition · edge reconstruction · density functional theory

Graphene has attracted extensive research interests recently due to its outstanding chemical, mechanical, and electronic properties and numerous potential applications.[1−5] The controlled synthesis of graphene is a fundamental step toward the industrial realization of these applications. Especially, high-quality graphene in large area is crucial for graphene device applications. Among various techniques of graphene production, the chemical vapor deposition (CVD) growth on the transition metal surface is the most promising approach for achieving this goal. It has been demonstrated that many transition metals, such as Rh,[6] Ru,[7] Ir,[8] Ni,[9,10] Pt,[11] Pd,[12] Cu,[13] *etc.*, can be used as catalysts for graphene CVD growth. Among them, Cu was broadly recognized as the best catalyst for large-area, high-quality, single-layer graphene synthesis.[13,14] While, to date, there is very little knowledge about why Cu is better than others for catalyzing graphene CVD growth.

Unlike the case of Ni, carbon has extremely low solubility in Cu bulk, and thus the graphene CVD growth on Cu is a pure surface process.[15−18] Considering the very low diffusion barrier of C atoms on the Cu surface,[19] the graphene growth should be limited by incorporating carbon atoms onto the edges of graphene islands. To understand the growth of graphene at the atomic scale, the detailed process of C atoms incorporating onto an edge of a growing graphene island is of particular importance. Experimentally, a large number of observations have shown that the dominating edge type of the growing graphene islands on the Cu surface is zigzag (ZZ).[20−22] On the basis of the well-known theory of crystal growth that *the faster growing edges would quickly disappear*,[23] this indicates that the armchair (AC) graphene edge should grow much faster than the ZZ one. To figure out the growth rates of various graphene edges, its edge structure must be determined in advance, which is the main motivation of this investigation.

The freestanding graphene edges possess very high formation energy, 13.46 and 10.09 eV/nm (or 3.35 and 2.18 eV/edge carbon atom) for ZZ and AC edges, respectively.[24] To lower the edge formation energies, the AC edge in vacuum is found to be self-passivated by triple C≡C bonds and the very active ZZ edge tends to be geometrically reconstructed into a chain of adjacent pentagon|heptagon (5|7) pairs.[25,26] Once placed on a transition metal surface

* Address correspondence to tcfding@inet.polyu.edu.hk, tctaoxm@inet.polyu.edu.hk, xschen@mail.sitp.ac.cn.

Received for review January 11, 2012 and accepted March 14, 2012.

Published online March 14, 2012
10.1021/nn300726r

TABLE 1. Graphene Edge Formation Energy (in eV/nm) in Vacuum and on Several Metal Surfaces, Where AC and ZZ Represent the Armchair and Zigzag Edges, Respectively

	None	Au(111)	Cu(111)	Ni(111)	Co(111)	Rh(111)	Ru(0001)
AC	10.09	9.87	7.41	4.55	5.34	4.93	4.97
ZZ	13.46	9.45	6.84	4.15	4.54	4.14	4.05

which is chemically very active, a graphene edge would be simultaneously passivated by the metal substrate due to the strong binding between the metal surface and the edge carbon atoms, and thus edge reconstruction is not favorable in energy (see following discussions). For example, on Ni(111), Co(111), Ru(0001), and Rh(111) surfaces, we find that the formation energies (see Table 1) are dramatically lowered by over 50% to 4.0−5.0 eV/nm or ∼1.0 eV/edge atom. In contrast, the formation energies of graphene edges on Cu(111) and Au(111) surfaces, in particular, for the AC edge, do not change much. For example, the formation energies of AC/ZZ edges on Cu(111) and Au(1111) surfaces are 7.41/6.84 and 9.87/9.45 eV/nm, respectively. On the basis of the interaction strength of graphene−metal, these catalyst surfaces can be classified into two groups: inert ones like Cu(111) and Au(111) and active ones like Ni(111), Co(111), Ru(0001), and Rh(111) surfaces. Such classification is in agreement with recent results calculated by Yuan *et al*.[27]

The high formation energies of graphene edges on Cu(111) and Au(111) surfaces imply that these edges are not efficiently passivated. Graphene CVD growth mostly occurs at the temperature of $T \sim 1000$ °C, which is high enough to activate the fast diffusion of metal adatoms on metal surfaces. Hence it is very possible for the active graphene edge to be passivated by these metal adatoms. Here we present a comprehensive study on the stability of several graphene edge configurations on Cu(111) and other metal surfaces by using the density functional theory (DFT) calculations. It is found that the termination of the AC edge by isolated Cu atoms is energetically most preferred while the ZZ edge tends to keep its pristine structure. Futher investigation shows that the Cu atom passivation on the AC sites greatly reduces the barrier of incorporating carbon atoms onto the AC edge and results in a fast growth of the AC edge on the Cu surface. As a consequence, on the basis of the classical theory of crystal growth, the ZZ edge should be the dominate edge of growing graphene islands.

RESULTS AND DISCUSSION

We first consider the stability of various potential graphene edges on the Cu(111) surface. It is well-known that the graphene nucleation tends to be initiated near a step on a metal surface.[24,28−30] Thus, here we consider a graphene nanoribbon (GNR) with one of its edges attached to a metal step of the Cu surface to model the growing graphene. Another edge of the GNR on the flat Cu(111) surface is active for the incorporation of C atoms. In this calculation, a few potential graphene edge configurations on the Cu surface, inculding of pristine, reconstructed, and Cu-terminated ones, have been considered. The optimized structures are shown in Figure 1 and Figure S1 in the Supporting Information. It can be seen that the binding position of AC GNRs on the Cu step is much higher than that of ZZ GNRs. Such a difference stems from the GNRs' electronic edge states. Each C atom of the AC edge has one dangling σ bond due to the self-passivation effect,[25] and thus it prefers to bond to one metal atom of step only. In contrast, a C atom of the ZZ edge has two active unpaired electrons,[27] and therefore, it tends to bond to two metal atoms, one belongs to the step and another one belongs to the flat surface.

It is well-known that a pristine ZZ edge of graphene is unstable and thus tends to be reconstructed into a linear pentagon−heptagon (5|7) chain in vacuum.[25,26] Very surprisingly, our calculation shows that all reconstructed ZZ/AC edges on the Cu surface are less stable than the pristine one (see Figure S1 of Supporting Information). This stems from the fact that the carbon atoms on the reconstructed graphene edges weakly bond to the Cu surface because of the self-passivation.[31] Therefore, we only consider the pristine AC or ZZ edge in the following discussions.

Beyond these reconstructed edges, the pristine graphene edges might be terminated by thermally activated metal atoms. Four types of Cu-terminated graphene edges, including of AC-Cu-I, AC-Cu-II, ZZ-Cu-I, and ZZ-Cu-II, have been considered in the present study (see Figure 1). AC-Cu-I/ZZ-Cu-I is the AC/ZZ graphene edge terminated by isolated Cu atoms (Figure 1b,e), and AC-Cu-II/ZZ-Cu-II is the AC/ZZ graphene edge terminated by a linear Cu chain (Figure 1c,f). The formation energies (E_f) of Cu-terminated graphene edges are defined as

$$E_f = (E_T - E_{GNR} - E_S - N_{Cu} \times \varepsilon_{Cu})/L \qquad (1)$$

where E_T, E_{GNR}, and E_S are the energies of the GNR on the Cu surface, GNR, and Cu substrate, respectively; ε_{Cu} is the cohesive energy of Cu bulk in eV/atom, N_{Cu} is the number of terminating Cu atoms, and L is the length of GNR edge.

Interestingly, both types of Cu-terminated AC graphene edges are more stable than the pristine one, as shown in Figure 1a−c. Their formation energies are 0.54 and 0.48 eV/nm lower than that of the pristine AC edge, respectively. Among them, the isolated Cu atoms terminated one, AC-Cu-I is more stable than AC-Cu-II, which is the graphene edge terminated by the linear Cu chain. In sharp contrast, the pristine edge is

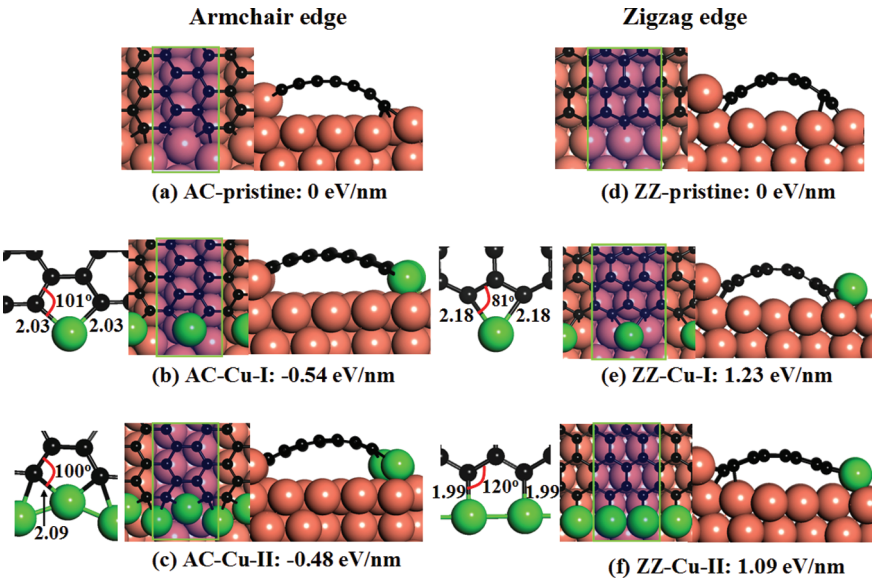

Figure 1. Top and side views of the optimized armchair (AC) and zigzag (ZZ) graphene edge configurations on a Cu(111) surface. The relative formation energies of each structure relative to the pristine AC/ZZ edge are shown. (a,d) Pristine AC/ZZ graphene edge; (b,e) AC/ZZ graphene edges terminated by isolated Cu atoms (labeled by AC-Cu-I/ZZ-Cu-I); (c,f) AC/ZZ graphene edges terminated by linear Cu chain (labeled by AC-Cu-II/ZZ-Cu-II). Small black and large yellow balls represent C and Cu atoms, respectively. The Cu atoms that terminate the graphene edges are highlighted by green. The rectangles in all panels denote the unit cells used in calculations.

energetically the most favorable structure among all ZZ edges. The formation energies of both ZZ-Cu-I and ZZ-Cu-II edges are more than 1.0 eV/nm higher than the pristine one. The effect of GNR width was tested by using wider GNRs to repeat these calculations (see Figure S2 of Supporting Information). The result shows that increasing the width of GNRs on the Cu surface only results in a minor change of the formation energies and their order does not change at all. This indicates that the curvature energy of the bent GNRs only contributes a minor fraction to the edge formation energies. The high stability of the Cu-terminated AC graphene edge is mainly attributed to the optimum geometry for the GNR–Cu interactions. For the Cu-terminated AC graphene edge, the C–C–Cu bond angles (101° and 100°, as shown in Figure 1b,c) are close to the standard sp^2 bond angle in graphene (120°). In contrast, although the Cu passivation also leads to the reduction of ribbon height, the C–C–Cu bonding angle of ZZ-Cu-I (81°, as shown in Figure 1e) is far from that in graphene, and thus the binding of the Cu atom to a ZZ edge is less stable than that on the AC edge. The ZZ-Cu-II (see Figure 1f) has the appropriate bond angle (120°) and shorter Cu–C bond length (1.99 Å), but, on average, each passivating Cu atom only bonds to one C atom. The formation of one Cu–C bond cannot afford the energy penalty of moving a Cu atom from bulk to the surface (~1.4 eV/atom).

The above results suggest that the Cu-terminated graphene AC edge is energetically preferred because the passivation with Cu atoms releases sufficient energy to compensate the energy cost of drawing Cu

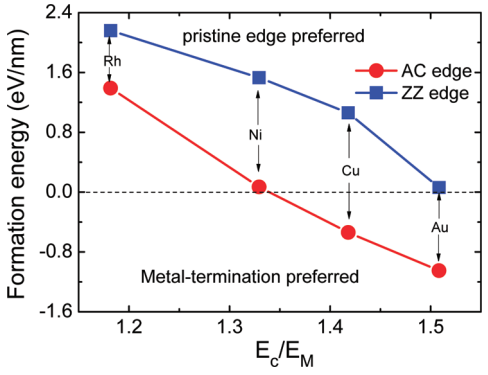

Figure 2. Formation energies of metal-terminated graphene edges (AC-Cu-I/ZZ-Cu-II) on Au(111), Cu(111), Ni(111), and Rh(111) surfaces as a function of relative binding interaction E_C/E_M; E_C and E_M are the adsorption energy of a carbon atom on metal surfaces and the cohesive energy of bulk metals, respectively.

atoms from bulk to the surface. In another word, whether a metal-terminated graphene edge is stable or not depends on the competition between metal–C and metal–metal interactions. To verify this assumption, four different metal surfaces, including Au(111), Cu(111), Ni(111), and Rh(111), are carefully studied. These four metal surfaces represent typical catalytic surfaces with different C–metal interactions: Au is very inert, Cu is slightly active, Ni is active, and Rh is very active. The order of interaction strengths between C and these metal surfaces is Rh > Ni > Cu > Au.[32,33]

As an indicator of the competition between metal–C and metal–metal interactions,[33,34] we have calculated the ratio, E_C/E_M, where E_C and E_M are the adsorption energy of a carbon atom on metal surfaces and the

cohesive energy of bulk metals, respectively. The formation energies *versus* E_C/E_M for the four representive metals are ploted in Figure 2 (detailed data are listed in Table S1 of Supporting Information). It is found that the metal-terminated AC graphene edge is preferred on both Au and Cu surfaces but not preferred on both Ni and Rh surfaces. For all of these metal surfaces, the metal-terminated ZZ graphene edge is energetically unfavorable. It is prominent that there is a strong correlation between the formation energies and E_C/E_M, that the larger the E_C/E_M, the lower the formation energy. The fitting lines show that the metal-terminated AC edge is stable when the E_C/E_M is larger than 1.33, while the stable metal-terminated ZZ edge requires E_C/E_M to be larger than 1.51. However, most metals have ratios smaller than 1.51, thus the metal-terminated ZZ graphene edge is difficult to be observed in experiments.

On the basis of the above analysis, the metal-terminated AC edge is energetically favorable on the Cu(111) surface but the ZZ edge tends to keep its pristine form. As expected in the aforementioned discussion, the AC edge should grow faster than the ZZ edge. It is common knowledge that edge passivation normally hinders addition of atoms and thus may slow the graphene growth rate. So how does the metal passivation affect the addition of C atoms onto a growing graphene edge?

To further understand the effect of passivating Cu atoms on the graphene growth, the detailed processes of incorporating carbon atoms onto AC and ZZ edges are studied, respectively. In most experiments of graphene CVD growth, the graphene feedstock pressure is very low (10^{-3} Torr or lower)[35] and thus the concentrations of C precursor on metal surfaces must be also very low. Experimentally, methane (CH_4), which has one C atom per molecule, is one of the most used feedstocks, especially for graphene growth on the Cu surface. The direct CH_4 decomposition releases C monomers on metal surfaces. Hence, the C monomer should be the most important C precursor in the graphene growth on the Cu surface. Certainly, during graphene growth, there is the probability of forming small C clusters by the coalescence of the C monomers.[33] As a kinetic process, the concentration of C_N clusters should be proportional to the rate of N C monomers meeting on the metal surface or

$$\rho_N \sim (\rho_1)^N \qquad (2)$$

where ρ_N and ρ_1 are the concentrations of C_N and carbon monomer, respectively. Equation 2 indicates that the larger is the cluster, the lower is the concentration. Thus, the graphene growth on the Cu surface should be mainly determined by the incorporation of C monomers (C_1) and the incorporation of small C clusters; especially, the C dimer may play a secondary role.

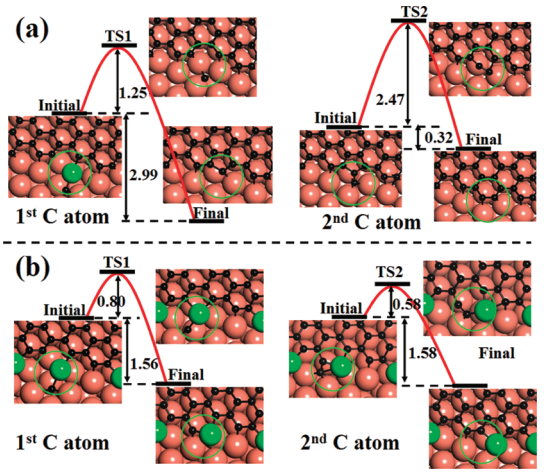

Figure 3. Repeatable cycles of incorporating two C atoms onto (a) pristine and (b) Cu-termianted armchair graphene edges on the Cu(111) surface. The circled regions represent the growth site. All of the energy differences are in the unit of eV.

For the growth of the AC edge, a repeatable cycle of graphene growth includes the addition of two C atoms in sequence (Figure 3a). In order to provide a reference, we first investigate the incorporation of two carbon monomers onto the pristine AC graphene edge on the Cu(111) surface. As shown in Figure 3a, once the first C atom reaches an AC site, one Cu atom is drawn out of the Cu(111) surface and leads to the formation of bridged C−Cu−C (or called bridged metal (BM) structure as in ref 34). The side view of the BM structure is shown in Figure S3a of Supporting Information. Such a process has been comprehensively explored by Wu *et al.*[34] The position exchange between the bridged Cu atom and the C atom is required to accomplish the attachment of the first C atom onto the graphene edge. The calculated barrier of the exchange is 1.25 eV. The optimized final structure has a pentagon on the AC edge and the Cu atom was drawn back to its original position. The incorporation of the first C atom is highly exothermic with a energy release of 2.99 eV. Owing to the high activity of the edge C atom in the pentagon, the second C atom is attached to the edge site of the pentagon with a negligible barrier, and the BM structure does not appear during the attachment. Then an extra step is required to transfer the pentagon plus dangling C formation to a new hexagon on the pristine AC edge and accomplish a cycle of growth. As shown in Figure 3a, healing the pentagon can be achieved by rotating the dangling C−C bond, and the barrier is substantial, 2.47 eV. In conclusion, during a cycle of C addition, the threshold step is the structure transformation and the threshold barrier is 2.47 eV.

Next, let us consider the incorporation of two carbon atoms on a Cu-terminated AC edge. As there is already an extra Cu atom appearing near the AC site, no further Cu atom is drawn out during the addition of both C atoms (see Figure 3b and Figure S3b). Similar to the

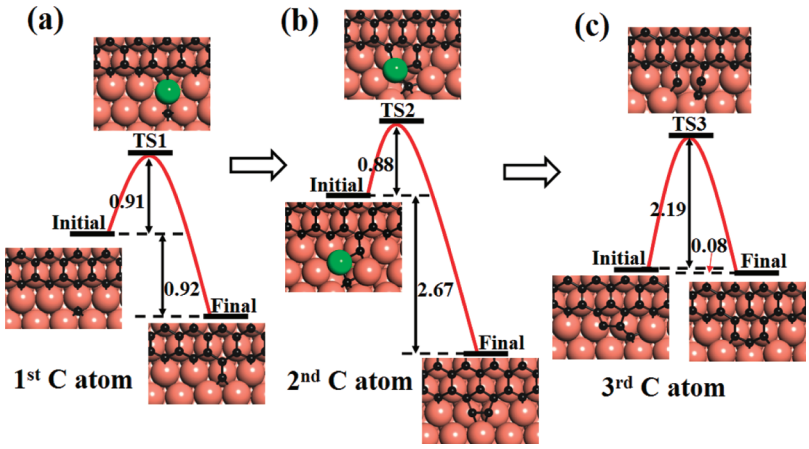

Figure 4. Incorporation processes of three carbon atoms onto the ZZ graphene edge on the Cu surface. The barriers (in eV) of incorporating (a) the first, (b) the second, and (c) the third carbons atoms have been listed, and top view of the initial, transition state (TS), and final structures of incorporating each C atom into the graphene edge is shown. The green balls represent the bridged Cu atom between C atoms. All of the energy differences are in the unit of eV.

incorporation of carbon atoms onto the pristine AC edge, the BM structure is formed at the arrival of the first C atom. A quite low barrier, 0.80 eV, is required to anchor the first C atom onto the graphene edge by the position exchange between the Cu atom and the C atom. As shown in Figure 3b, the anchored C atom and the terminating Cu atom form a hexagon at the AC edge, which is very different from that on the pristine edge. The arrival of the second C atom forms a triangle with the first C atom and the passivating Cu atom. Then the unstable triangle opens to form a heptagon ring on the graphene edge. Such a heptagon structure is just a transition state (TS) and can be transformed into a hexagon ring of C atoms. The barrier of the transformation is merely 0.58 eV. Hence, for the C addition on a Cu-terminated AC edge, the existence of the Cu atom greatly reduces the threshold barrier from 2.47 to 0.8 eV and the threshold step becomes the incorporation of the first C atom.

Different from the AC edge, the pristine graphene ZZ edge is energetically more favorable than others. Thus, only C addition onto the pristine ZZ edge is considered here. To form a new hexagon on the ZZ edge, the incorporation of three C atoms onto the edge in sequence is required. Similar to the growth of the pristine AC edge, a BM structure (side view of this structure is shown in Figure S3c) is formed when the first C atom arrives at the ZZ edge (Figure 4a). The barrier of the first C atom attachment is 0.91 eV (Figure 4a). The arrival of the second C atom also excites the BM structure, and the drawn Cu atom and the first C atom form a pentagon at the ZZ edge (Figure 4b and Figure S3d). Then the following position exchange between the Cu and the second C atom leads to a C pentagon, and the corresponding barrier is 0.88 eV. The incorporation of the third C atom is required to form a complete hexagon at the ZZ edge. During the addition of the third C atom, no BM formation is shown, and thus the third C atom can be directly added onto a vortex of the pentagon. To form a perfect new hexagon at the ZZ edge, a structural transformation from the "pentagon + dangling C" formation into a hexagon is required. It is important to note that there are two possible transformation paths to heal the "pentagon + dangling C" formation. Path (i) is shown in Figure 4c that the transformation can be achieved by rotating the dangling C−C bond by overcoming a barrier of 2.19 eV. Path (ii) is assisted by an additional Cu atom. As shown in Figure S4 of Supporting Information, the attachment of the third C atoms leads to an active armchair-like site and the accommodation of a Cu atom into the site is slightly favorable (relative formation energy is −0.13 eV). The attachment of the additional Cu atom does not result in any deduction of the defect healing barrier on the ZZ edge because the Cu atom is far from the rotating C−C bond (as shown in Figure S5 of Supporting Information; the barrier is 2.21 eV). Therefore, both paths show that the incorporation of the third C atom is the threshold step.

Because C monomers may aggregate into small C clusters in a small probability on the metal surface before they are incorporated onto the graphene edge, the cluster effect on the barrier of C incorporation was studied. The processes of the most probable C cluster, carbon dimer (C_2), incorporated onto pristine and Cu-passivated graphene edges are shown in Figure S6 of Supporting Information. The threshold barriers are 2.47 and 0.84 eV, respectively. Therefore, the passivating Cu atoms play a very similar role in greatly lowering the threshold barriers of incorporating C_1 and C_2 precursors onto the AC edge. For the incorporation of a C_2 onto the pristine zigzag edge, the addition of one C_2 leads to a pentagon formation on the ZZ edge first. Therefore, the threshold step is the healing of defects, same as that shown in Figure 4c.

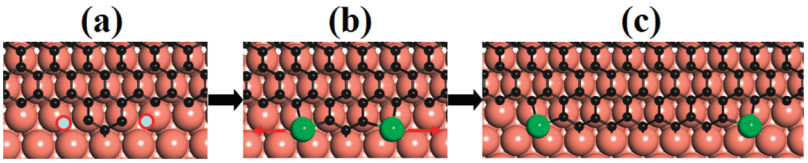

Figure 5. Growth of the graphene zigzag (ZZ) edge on Cu(111) surface: (a) formation of a hexagon at the ZZ edge induces two active AC-like sites; (b) Cu atoms attach at the two active AC-like sites as the active growth sites; (c) continuous incorporation of C atoms at both AC-like sites leads to the formation of a new ZZ chain on the graphene growth front.

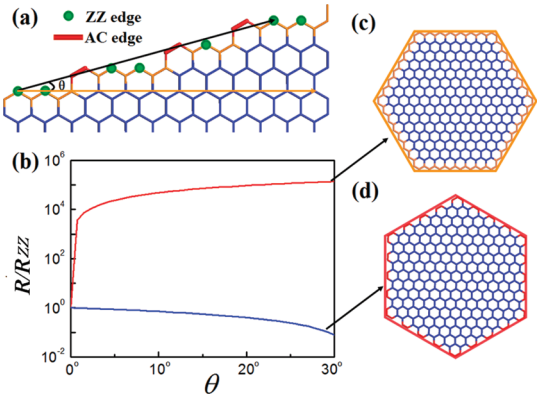

Figure 6. (a) Schematic illustration of an arbitrary graphene edge with the tilt angle θ, $0° \le \theta \le 30°$. (b) Ratio of growth rates (R/R_{ZZ}) of an arbitrary graphene edge and zigzag edge as a function of θ; the blue and red lines represent the results of AC sites on the edge without and with the Cu termination, respectively. The morphologies of growing graphene islands obtained by the kinetic Wulff plots (see Figure S7 of Supporting Information) with (c) and without (d) considering passivation of AC sites during growth.

On the basis of these discussions, we conclude that the passivating Cu atom plays an exact same role in the addition of both C monomer and dimer.

When a new hexagon is formed at the ZZ edge, two active AC-like sites appear (Figure 5a). Then the active AC-like sites will be passivated by Cu atoms (see Figure 5b), and this process is very energetically favorable. Owing to the low barrier of C incorporation, the subsequent growth will be dominated by continuous deposition of C atoms onto both Cu-terminated AC sites (see Figure 5c).

We now turn to investigate the growth rate of an arbitrary graphene edge which has a tilt angle θ from the ZZ direction. As shown in Figure 6a, such a graphene edge mixes both AC-like and ZZ-like sites. Denoting the concentrations of AC-like and ZZ-like sites as c_{AC} and c_{ZZ}, respectively, the growth rate R of an arbitrary edge can be expressed as

$$R = c_{AC} \times R_{AC} + c_{ZZ} \times R_{ZZ} \quad (3)$$

As detailed in ref 36, $c_{AC} = (4/\sqrt{3})\sin(\theta)$ and $c_{ZZ} = 2\sin(30° - \theta)$ (Figure 6a). Thus the growth rate can be rewritten as

$$R(\theta) = (4/\sqrt{3}) \times R_{AC} \times \sin(\theta) + 2 \times R_{ZZ} \times \sin(30^\circ - \theta) \quad (4)$$

Kinetically, the rate of C atoms attaching to ZZ-like or AC-like sites can be considered as a function of the threshold barrier, E_b:

$$R \propto \exp(-E_b/kT) \quad (5)$$

where k is the Boltzmann constant and T is the temperature of graphene growth. Choosing the typical temperature of graphene CVD growth, $T = 1200$ K, as an example, the ratios of $R(\theta)/R_{ZZ}$ of graphene growth on the Cu(111) surface as functions of θ, with and without considering the Cu atom passivation on AC sites, are presented in Figure 6b. Without considering the passivation effect, because the threshold barrier of incorporating C atoms onto a prisine ZZ edge (2.19 eV) is lower than that onto a prisine AC edge (2.47 eV), the growth rate monotonically decreases with θ. As a consequence, slowly growing AC edge (corresponding to θ = 30°) should dominate the edge of growing graphene islands (see Figure 6d and Figure S7 of Supporting Information). Certainly, this contradicts most experimental observations.[19−21] In contrast, considering the Cu atom passivation, the barrier of incorporating C atoms onto an AC edge (0.8 eV) is far lower than that onto a ZZ edge, and the growth rate monotonically increases with θ. In eq 3, neglecting the very slow growth on the ZZ sites, the growth rate of an arbitrary edge is proportional to the concentration of AC sites or $R(\theta) \sim \sin(\theta)$. This is similar to the screw dislocation theory of carbon nanotube growth.[37] The result leads to a real experimental landscape that the active AC edges grow very rapidly and gradually disappear, and the inert ZZ edges grow very slowly and eventually dominate the circumference of a growing graphene island (Figure 6c and Figure S7 of Supporting Information).

CONCLUSIONS

In summary, we have performed a detailed theoretical investigation on the structural stability and growth kinetics of graphene edges on the Cu(111) surface. The Cu atom passivated armchair (AC) edge presents superior stability over other potential structures. Such a stable edge formation is attributed to the competition between the metal−C and metal−metal interactions. Futhermore, the growth kinetic study shows that the Cu termination on the graphene AC edge significantly reduces the threshold barrier of

incoporating carbon atoms from 2.47 to 0.80 eV and leads to a fast growth rate of the AC edge. This is in good agreement with broad experimental observations that the zigzag (ZZ) edge dominates the circumference of growing graphene islands on the Cu surface.

METHODS

All calculations in the present study were performed by using the density functional theory (DFT) as implemented by the Vienna Ab Initio Simulation Package (VASP).[38,39] The exchange-correlation energy was described in the generalized gradient approximation (GGA) using the PBE functional.[40] The energy cutoff for the plane-wave expansion was set to 400 eV, using the projector-augmented wave (PAW) potentials[41] to describe the electron−ion interaction. The Monkhorst-Pack *k*-point mesh of $4 \times 2 \times 1$ was found to provide sufficient accuracy in the Brillouin zone integration. The geometry optimization was performed using the conjugate gradient scheme until the force acting on each atom is less than 0.01 eV/Å. The climbing image nudged elastic band (CI-NEB) method[42] was used for the transition state search and incorporation barrier determination of carbon atoms.

To investigate the interaction between graphene nanoribbons (GNRs) and metal surfaces, a three-layer metal slab with fixed bottom layer atoms was used to represent the metal surfaces, then the GNR was put on the metal surfaces (*e.g.*, Au(111), Cu(111), Ni(111), Ru(0001), and Rh(111)) with fully structural relaxations. The schematic models for GNR on the metal surface (zigzag and armchair GNRs on the Cu(111) surface) are shown in Figure S8 of Supporting Information. The repeated slabs were separated by more than 10 Å to eliminate their interactions, and the allowed lattice match of GNR−metal interfaces in the constructed slab models is smaller than 3%. On the basis of this model, the graphene edge formation energies, E_f, were calculated by the following formula

$$E_f = (E_M + E_{GNR} - E_{tot})/L \quad (6)$$

where E_{tot}, E_M, and E_{GNR} are the total energies of metal slab with GNR, supported metal surface, and freestanding GNR, respectively; L is the length of unit cell along the periodic direction of GNR.

The second model is used to study the possible graphene edges on the Cu(111) surface. It is a well-known fact that the graphene growth tends to begin at the metal step for most metal surfaces.[28−30] Thus, we have constructed the GNR with one edge attached to a metal step on the Cu(111) surface. Another edge of GNR was used to represent the growing front of graphene. To investigate the effect of ribbon length on the stability of graphene edges, we have considered two different lengths for both armchair and zigzag GNRs. They are 7.38 and 12.30 Å for armchair GNRs and 7.10 and 15.62 Å for zigzag GNRs. Various potential edge configurations of the front were considered, including of pristine, reconstructed, and Cu-terminated graphene edges (the optimized structures are shown in Figure 1, Figure S1, and Figure S2). The stepped Cu(111) surface is based on a three-layer slab model in which the bottom layer was fixed to mimic the bulk. The unit cells of the slab are 4.31 Å × 12.87 Å and 5.01 Å × 16.02 Å for the AC and ZZ graphene edges on the Cu surface, respectively. Similar models were used to investigate the edge stability of graphene on Au, Ni, and Rh surfaces, and the models of metal-terminated graphene edges on these surfaces are shown in Figure S9 of Supporting Information. The unit cells of AC GNRs on Au, Ni, and Rh surfaces are 8.65 Å × 18.47 Å, 4.29 Å × 12.71 Å, and 13.05 Å × 16.84 Å, respectively. For the ZZ GNRs on Au, Ni, and Rh surfaces, their unit cells are 4.99 Å × 14.70 Å, 4.98 Å × 15.96 Å, and 9.62 Å × 13.72 Å, respectively.

In order to model the kinetic process of incorporating carbon atoms into pristine or Cu-terminated AC edge, a larger surface slab with the unit cell of 17.22 Å × 12.87 Å was used in the present study. In the model, we consider the graphene edge with a step at the growth end (see Figure 3 and Figure S6). On the basis of this model, the incorporation of each of the two carbon atoms into the graphene edge will induce a new hexagon. Similarly, a metal slab with the unit cell of 10.02 Å × 16.02 Å was used to investigate the incorporation process of C atoms at the ZZ edge. To form a new hexagon ring, the incorporation of three C atoms onto the ZZ edge in sequence is required (see Figure 4). Owing to the large supercells, the *k*-point meshes used in the calculations are $1 \times 2 \times 1$ and $2 \times 1 \times 1$ for the C atom incorporating onto AC and ZZ edges, respectively.

Conflict of Interest: The authors declare no competing financial interest.

Acknowledgment. This work was supported in part by the State Key Program for Basic Research of China (2007CB613206), the National Natural Science Foundation of China (61006090, 10990104, and 60976092), and the Foundation of Shanghai Science and Technology Foundation (09DJ1400203, 10JC1416100, and 10510704700). Computational resources from the Shanghai Supercomputer Center and Tianjin are acknowledged.

Supporting Information Available: Optimized configurations of pristine and reconstructed armchair and zigzag graphene nanoribbons on the Cu surface; optimized configurations of long armchair and zigzag graphene nanoribbons on the stepped Cu(111) surface and their formation energies relative to the pristine GNR; side view of graphene edges with the bridged Cu atom on the Cu surfaces during the graphene growth; comparison of structural stability between pristine and Cu-terminated zigzag graphene edges with a C pentagon and dangling C atom; incorporation process of the third C atom onto the Cu-terminated zigzag graphene edge on the Cu(111) surface; repeatable cycles of C dimer onto pristine and Cu-terminated armchair graphene edges on the Cu(111) surface, respectively; evolution of edge circumference of the graphene island based on the crystal growth theory and the corresponding kinetic Wulff plots of graphene edges; top and side view of armchair and zigzag graphene nanoribbons on the Cu(111) surface; top and side view of armchair and zigzag metal-terminated graphene nanoribbons on Au, Ni, and Rh surfaces; a table for the formation energies of metal-terminated graphene edges relative to their pristine edge, the adsorption energies of C atom on metal surfaces, and the cohesive energies of metal bulk. This material is available free of charge *via* the Internet at http://pubs.acs.org.

REFERENCES AND NOTES

1. Geim, A. K.; Novoselov, K. S. The Rise of Graphene. *Nat. Mater.* **2007**, *6*, 183–191.
2. Dimiev, A.; Kosynkin, D. V.; Sinitskii, A.; Slesarev, A.; Sun, Z.; Tour, J. M. Layer-by-Layer Removal of Graphene for Device Patterning. *Science* **2011**, *331*, 1168–1172.
3. Wu, M. H.; Pei, Y.; Zeng, X. C. Planar Tetracoordinate Carbon Strips in Edge Decorated Graphene Nanoribbon. *J. Am. Chem. Soc.* **2010**, *132*, 5554–5555.
4. Geim, A. K. Graphene: Status and Prospects. *Science* **2009**, *324*, 1530–1534.
5. Li, Y. F.; Zhou, Z.; Shen, P. W; Chen, Z. F. Structural and Electronic Properties of Graphane Nanoribbons. *J. Phys. Chem. C* **2009**, *113*, 15043–15045.
6. Preobrajenski, A. B.; Ng, M. L.; Vinogradov, A. S.; Mårtensson, N. Controlling Graphene Corrugation on Lattice-Mismatched Substrates. *Phys. Rev. B* **2008**, *78*, 073401.

7. Marchini, S.; Günther, S.; Wintterlin, J. Scanning Tunneling Microscopy of Graphene on Ru(0001). *Phys. Rev. B* **2007**, *76*, 074429.
8. N'Diaye, A. T.; Bleikamp, S.; Feibelman, P. J.; Michely, T. Two-Dimensional Ir Cluster Lattice on a Graphene Moire on Ir(111). *Phys. Rev. Lett.* **2006**, *97*, 215501.
9. Zhang, Y.; Gomez, L.; Ishikawa, F. N.; Madaria, A.; Ryu, K.; Wang, C.; Badmaev, A.; Zhou, C. Comparison of Graphene Growth on Single-Crystalline and Polycrystalline Ni by Chemical Vapor Deposition. *J. Phys. Chem. Lett.* **2010**, *1*, 3101–3107.
10. Lee, Y.; Bae, S.; Jang, H.; Jang, S.; Zhu, S.-E.; Zhu, S. H.; Sim, S. H.; Song, Y. I.; Hong, B. H.; Ahn, J.-H. Wafer-Scale Synthesis and Transfer of Graphene Films. *Nano Lett.* **2010**, *10*, 490–493.
11. Sutter, P.; Sadowski, J. T.; Sutter, E. Graphene on Pt(111): Growth and Substrate Interaction. *Phys. Rev. B* **2009**, *80*, 245411.
12. Kwon, S.-Y.; Ciobanu, C. V.; Petrova, V.; Shenoy, V. B.; Bareño, J.; Gambin, V.; Petrov, I.; Kodambaka, S. Growth of Semiconducting Graphene on Palladium. *Nano Lett.* **2009**, *9*, 3985–3990.
13. Reddy, K. M.; Gledhill, A. D.; Chen, C. H.; Drexler, J. M.; Padture, N. P. High Quality, Transferrable Graphene Grown on Single Crystal Cu(111) Thin Films on Basal-Plane Sapphire. *Appl. Phys. Lett.* **2011**, *98*, 113117.
14. Gao, L.; Guset, J. R.; Guisinger, N. P. Epitaxial Graphene on Cu(111). *Nano Lett.* **2010**, *10*, 3512–3516.
15. Li, X. S.; Cai, W. W.; Colombo, L.; Ruoff, R. S. Evolution of Graphene Growth on Ni and Cu by Carbon Isotope Labeling. *Nano Lett.* **2009**, *9*, 4268–4272.
16. Zhang, W. H.; Wu, P.; Li, Z. Y.; Yang, J. L. First-Principles Thermodyamics of Graphene Growth on Cu Surfaces. *J. Phys. Chem. C* **2011**, *115*, 17782–17787.
17. Li, Z. C.; Wu, P.; Wang, C. X.; Fan, X. D.; Zhang, W. H.; Zhai, X. F.; Zeng, C. G.; Li, Z. Y.; Yang, J. L.; Hou, J. G. Low-Temperature Growth of Graphene by Chemical Vapor Deposition Using Solid and Liquid Carbon Source. *ACS Nano* **2011**, *5*, 3385–3390.
18. Van Wesep, R. G.; Chen, H.; Zhu, W. G.; Zhang, Z. Y. Stable Carbon Nanoarches in the Initial Stages of Epitaxial Growth of Graphene on Cu(111). *J. Chem. Phys.* **2011**, *134*, 171105.
19. Yazyev, O. V.; Pasquarello, A. Effect of Metal Elements in Catalytic Growth of Carbon Nanotubes. *Phys. Rev. Lett.* **2008**, *100*, 156102.
20. Tian, J. F.; Cao, H. L.; Wu, W.; Yu, Q.; Chen, Y. P. Direct Imaging of Graphene Edges: Atomic Structure and Electronic Scattering. *Nano Lett.* **2011**, *11*, 3663–3368.
21. Yu, Q.; Jauregui, L. A.; Wu, W.; Colby, R.; Tian, J.; Su, Z.; Cao, H.; Liu, Z.; Pandy, D.; Wei, D.; *et al.* Control and Characterization of Individual Grains and Grain Boundaries in Graphene Grown by Chemical Vapor Deposition. *Nat. Mater.* **2011**, *10*, 443–449.
22. Jauregui, L. A.; Cao, H.; Wu, W.; Yu, Q.; Chen, Y. P. Electronic Properties of Grains and Grain Boundaries in Graphene Grown by Chemical Vapor Deposition. *Solid State Commun.* **2011**, *151*, 1100–1104.
23. Sun, Q.; Yerino, C. D.; Leung, B.; Han, J.; Coltrin, M. E. Understanding and Controlling Heteroepitaxy with the Kinetic Wulff Polt: A Case Study with GaN. *J. Appl. Phys.* **2011**, *110*, 053517.
24. Gao, J. F.; Yip, J.; Zhao, J. J.; Yakobson, B. I.; Ding, F. Graphene Nucleation on Transition Metal Surface: Structure Transformation and Role of the Metal Step Edge. *J. Am. Chem. Soc.* **2011**, *133*, 5009–5015.
25. Koskinen, P.; Malola, S.; Häkkinen, H. Self-Passivating Edge Reconstruction of Graphene. *Phys. Rev. Lett.* **2008**, *101*, 115502.
26. Huang, J. Y.; Ding, F.; Yakobson, B. I.; Lu, P.; Qi, L.; Li, J. *In Situ* Observation of Graphene Sublimation and Multi-layer Edge Reconstructions. *Proc. Natl. Acad. Sci. U.S.A.* **2009**, *106*, 10103–10108.
27. Yuan, Q. H.; Gao, J. F.; Shu, H. B.; Zhao, J. J.; Chen, X. S.; Ding, F. Magic Carbon Clusters in the Chemical Vapor Deposition Growth of Graphene. *J. Am. Chem. Soc.* **2012**, *134*, 2970–2975.
28. Weatherup, R. S.; Bayer, B. C.; Blume, R.; Ducati, C.; Baehtz, C.; Schlögl, R.; Hofmann, S. *In Situ* Characterization of Alloy Catalysts for Low-Temperature Graphene Growth. *Nano Lett.* **2011**, *11*, 4154–4160.
29. Coraux, J.; N'Diaye, A. T.; Engler, M.; Busse, C.; Wall, D.; Buckanie, N.; Heringdorf, F.-J. M.; Gastel, R. v.; Poelsema, B.; Michely, T. Growth of Graphene on Ir(111). *New J. Phys.* **2009**, *11*, 023006.
30. Wood, J. D.; Schmucker, S. W.; Lyons, A. S.; Pop, E.; Lyding, J. W. Effect of Polycrystalline Cu Substrate on Graphene Growth by Chemical Vapor Deposition. *Nano Lett.* **2011**, *11*, 4547–4554.
31. Yuan, Q. H.; Hu, H.; Gao, J. F.; Ding, F.; Liu, Z. F.; Yakobson, B. I. Upright Standing Graphene Formation on Substrates. *J. Am. Chem. Soc.* **2011**, *13*, 16072–16079.
32. Ding, F.; Larsson, P.; Larsson, J. A.; Ahuja, R.; Duan, H. M.; Rosén, A.; Bolton, K. The Importance of Strong Carbon–Metal Adhesion for Catalytic Nucleation of Single-Walled Carbon Nanotubes. *Nano Lett.* **2008**, *8*, 463–468.
33. Chen, H.; Zhu, W. G.; Zhang, Z. Y. Contrasting Behavior of Carbon Nucleation in the Initial Stages of Graphene Epitaxial Growth on Stepped Metal Surfaces. *Phys. Rev. Lett.* **2010**, *104*, 186101.
34. Wu, P.; Zhang, W. H.; Li, Z. Y.; Yang, J. L.; Hou, J. G. Coalescence of Carbon Atoms on Cu(111) Surface: Emergence of a Stable Bridging-Metal Structure Motif. *J. Chem. Phys.* **2010**, *133*, 071101.
35. Vlassiouk, I.; Regmi, M.; Fulvio, P.; Dai, S.; Datskos, P.; Eres, G.; Smirnov, S. Role of Hydrogen in Chemical Vapor Deposition Growth of Large Single-Crystal Graphene. *ACS Nano* **2011**, *5*, 6069–6076.
36. Liu, Y. Y.; Dobrinsky, A.; Yakobson, B. I. Graphene Edge from Armchair to Zigzag: The Origins of Nanotube Chirality? *Phys. Rev. Lett.* **2010**, *105*, 235502.
37. Ding, F.; Harutyunyan, A. R.; Yakobson, B. I. Dislocation Theory of Chirality-Controlled Nanotube Growth. *Proc. Natl. Acad. Sci. U.S.A.* **2009**, *106*, 2506–2509.
38. Blöchl, P. E. Projector Augmented-Wave Method. *Phys. Rev. B* **1994**, *50*, 17953–17979.
39. Kresse, G.; Furthmüller, J. Efficient Iterative Schemes for *Ab Initio* Total-Energy Calculations Using a Plane-Wave Basis Set. *Phys. Rev. B* **1996**, *54*, 11169–11186.
40. Perdew, J. P.; Burke, K.; Ernzerhof, M. Generalized Gradient Approximation Made Simple. *Phys. Rev. Lett.* **1996**, *77*, 3865–3868.
41. Kresse, G; Joubert, D. From Ultrasoft Pseudopotentials to the Projector Augmented-Wave Method. *Phys. Rev. B* **1999**, *59*, 1758–1775.
42. Henkelman, G.; Uberuaga, B. P.; Jónsson, H. A Climbing Image Nudged Elastic Band Method for Finding Saddle Points and Minimum Energy Paths. *J. Chem. Phys.* **2000**, *113*, 9901.